IMPROVED GALLIUM NITRIDE AND ALUMINUM NITRIDE ELECTRONIC MATERIALS

W. D. Partlow (PI), W. J. Choyke, R. P. Devaty, John T. Yates, Jr., Karl-Heinz Bornscheuer, P. J. Chen, C. C. Cheng, M. L. Colaianni, H. Gutleben, S. R. Lucas, M. F. MacMillan

Annual Report for the period
February 20, 1991 to February 19, 1992

General Order No. I WGD-12523-CE

Contract No. F49620-91-C-0032

Air Force Office of Scientific Research
Bolling Air Force Base
Washington, DC 20332

Westinghouse STG
1310 Beulah Road
Pittsburgh, Pennsylvania 15235

IMPROVED GALLIUM NITRIDE AND ALUMINUM NITRIDE ELECTRONIC MATERIALS

W. D. Partlow (PI), W. J. Choyke, R. P. Devaty,
John T. Yates, Jr., Karl-Heinz Bornschauer,
P. J. Chen, C. C. Cheng, M. L. Colaianni, H. Gutleben,
S. R. Lucas, M. F. MacMillan

Annual Report for the period
February 20, 1991 to February 19, 1992

General Order No.I WGD-12523-CE

Contract No. F49620-91-C-0032

Air Force Office of Scientific Research
Bolling Air Force Base
Washington, DC 20332

April 20, 1992

Westinghouse STC
1310 Beulah Road
Pittsburgh, Pennsylvania 15235

ABSTRACT

This report describes the progress in the first year of a three year program to improve the quality of gallium and aluminum nitride electronic materials. In this period the experimental apparatus for the ultrahigh vacuum characterization of nitride growth processes was upgraded to increase the capability for experimental control and characterization of growth surfaces. These improvements include the addition of a cooled atomic hydrogen source and a reverse view LEED apparatus. Vibrational studies of the methyl radical on Si(100) surfaces were completed, increasing the understanding of the kinetics and stability of this radical, important for understanding growth from alkyl precursors. Cathodoluminescence and infrared reflectometry measurements were performed on numerous samples of epitaxial aluminum nitride to build up a base for materials quality determination.

REPORT DOCUMENTATION PAGE

Form Approved
OMB No. 0704-0188

1. AGENCY USE ONLY (Leave blank)	2. REPORT DATE	3. REPORT TYPE AND DATES COVERED
		Annual Feb. 20, 1991 - Feb. 19, 1992

4. TITLE AND SUBTITLE
IMPROVED GALLIUM NITRIDE AND ALUMINUM NITRIDE ELECTRONIC MATERIALS

5. FUNDING NUMBERS
F49620-91-C-0032

6. AUTHOR(S)
W. D. Partlow (PI), W. J. Choyke, R. P. Devaty, John T. Yates, Jr., Karl-Heinz Bornschauer, P. J. Chen, C. C. Cheng, M. L. Colaianni, H. Gutleben, S. R. Lucas, M. F. MacMillan

7. PERFORMING ORGANIZATION NAME(S) AND ADDRESS(ES)
Westinghouse STC
1310 Beulah Road
Pittsburgh, PA 15235-5098

8. PERFORMING ORGANIZATION REPORT NUMBER
92-9SB2-ALGAN-R1

9. SPONSORING/MONITORING AGENCY NAME(S) AND ADDRESS(ES)
Air Force Office of Scientific Research
Bolling Air Force Base
Washington, DC 20332

10. SPONSORING/MONITORING AGENCY REPORT NUMBER
2306 B1

11. SUPPLEMENTARY NOTES

12a. DISTRIBUTION/AVAILABILITY STATEMENT
unlimited

12b. DISTRIBUTION CODE

13. ABSTRACT (Maximum 200 words)

This report describes the progress in the first year of a three-year program to improve the quality of gallium and aluminum nitride electronic material. In this period the experimental apparatus for the ultrahigh vacuum characterization of nitride growth processes was upgraded to increase the capability for experimental control and characterization of growth surfaces. These improvements include the addition of a cooled atomic hydrogen source and a reverse view LEED apparatus. Vibrational studies of the methyl radical on Si(100) surfaces were completed, increasing the understanding of the kinetics and stability of this radical, important for understanding growth from alkyl precursors. Cathodoluminescence and infrared reflectometry measurements were performed on numerous samples of epitaxial aluminum nitride to build up a base for materaials quality determination.

14. SUBJECT TERMS	15. NUMBER OF PAGES
	41
	16. PRICE CODE

17. SECURITY CLASSIFICATION OF REPORT	18. SECURITY CLASSIFICATION OF THIS PAGE	19. SECURITY CLASSIFICATION OF ABSTRACT	20. LIMITATION OF ABSTRACT
Unrestricted	Unrestricted	Unrestricted	

1. PROGRAM OBJECTIVE AND OVERVIEW

The objective of the program is to improve the electronic quality of Group III Nitrides through understanding and control of material growth processes. The program concentrates on the growth of gallium and aluminum nitrides from alkyl precursors such as trimethl and triethyl gallium. The kinetics of adsorption/desorption and reaction of monolayers on growth surfaces are measured by ultrahigh vacuum techniques, including temperature programmed desorption (TPD), and quantitative kinetic uptake measurements.

These measurements, and the character of the deposited layers, provide insight into the issues associated with obtaining desirable material properties such as good nitrogen stoichiometry and low carbon impurity. The are relevant to the understanding and control of CVD and atomic layer epitaxy growth techniques, and to MBE growth to a lesser extent.

In addition to the in-situ characterization techniques associated with the UHV experiments, the program contains a research task to develop an understanding of Group III nitride materials through low temperature cathodoluminescence (LTCL) and Fourier transform infrared (FTIR) reflectance measurements. The former technique focuses on electronic structure of the material through measurements of the exciton and intra-band emission spectra, while the latter techniques provides basic structural information via infrared vibrational studies.

2. PROGRAM STATUS

In the surface chemistry area, we have carried out the following activities:

a. completed survey experiments on growth kinetics,
b. upgraded the growth kinetics reactor to include:
   - improved pumping and gas handling,
   - reverse view LEED for structural characterization,
   - novel source of cool atomic hydrogen atoms,
c. completed vibrational studies of methyl radicals on Si(100) surfaces.

Survey experiments were carried out with trimethyl aluminum deposition precursors to define the adsorption and reaction kinetics experiments and to determine equipment requirements. We also carried out experiments with aluminum chloride precursors. The existing apparatus was found to require significant modifications for the experiments planned on this program. Heating of the adsorbed layers by the hot filament which produces atomic hydrogen was found to be excessive, so a new, cryogenically cooled source of atomic hydrogen was designed. The gas dosing manifold was inadequate, and was also redesigned. We concluded that structural characterization was needed, in addition to the existing elemental (Auger) characterization. Figure 1 shows a schematic of the upgraded experimental apparatus, compared to the original version. The modifications have been completed, and

Figure 1a: Schematic of the upgraded UHV growth kinetics experimental apparatus.

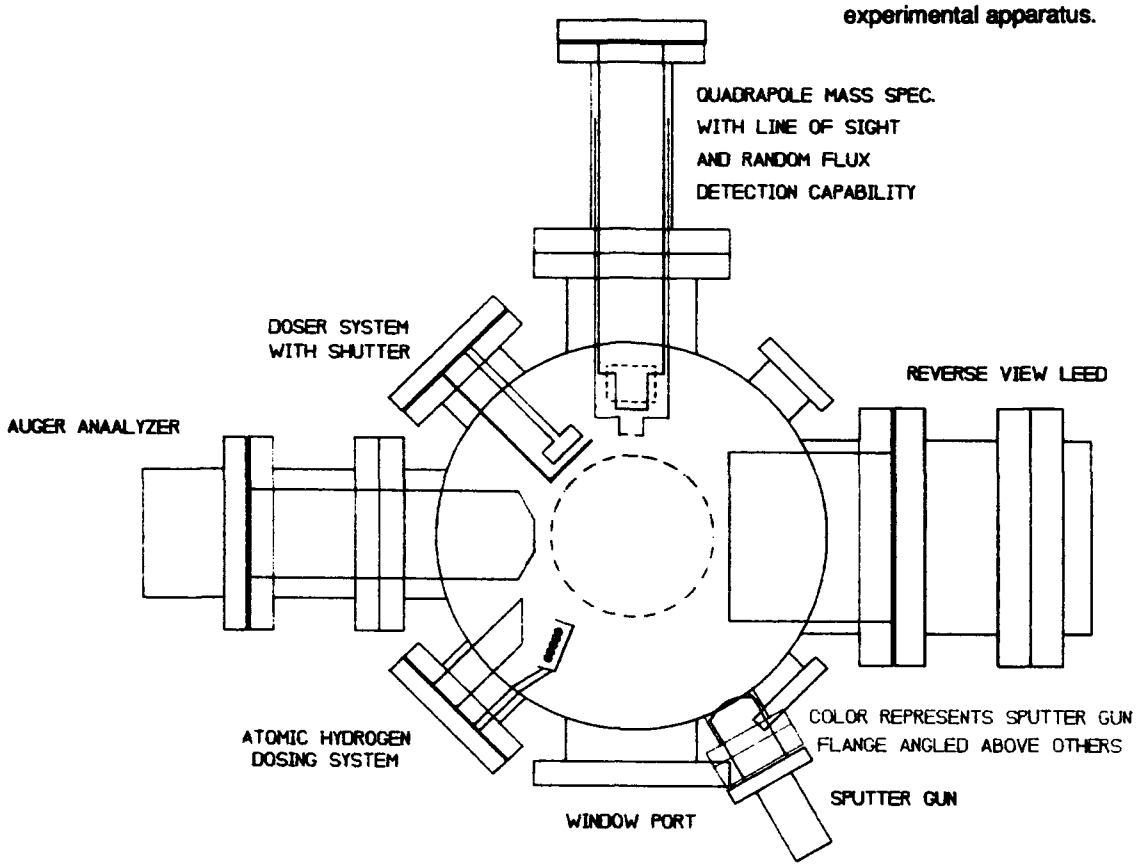

Figure 1b: Schematic of the original UHV growth kinetics experimental apparatus, shown for comparison.

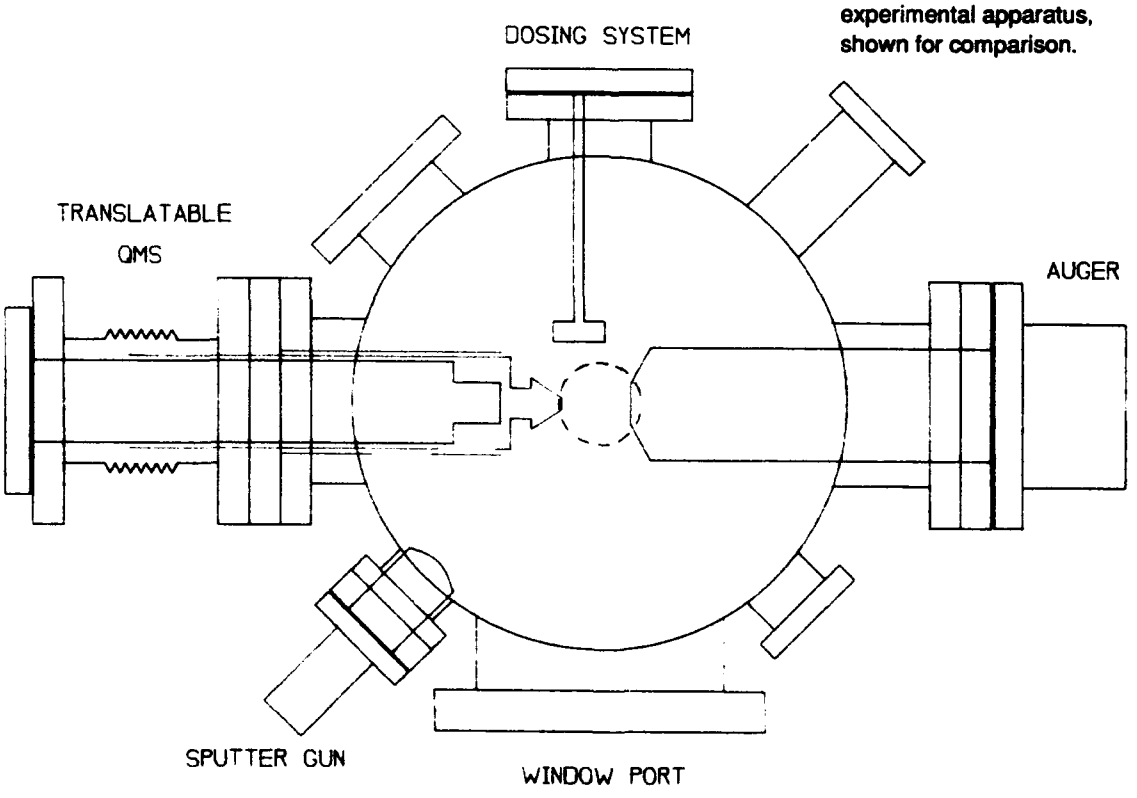

experiments are underway to characterize the modified equipment and to carry out growth kinetics experiments.

On a separate apparatus we obtained a significant level of understanding of the kinetics and stability of the methyl radical on Si(100) surfaces, by carrying out vibrational studies of adsorbed species.[1] This builds on the work on the dissociative adsorption of CH_3I that we began in the former program.[2] These studies spectroscopically tracked the adsorption, dissociation, and thermal decomposition of the methyl radical. The ranges of stability were determined, and the dissociated species were detected and identified. For the reader who seeks an in-depth technical presentation of this topic, we have included references 1 and 2 which, taken together, provide this information.

In the materials characterization effort, AlN and GaN epitaxial layers, grown by several techniques, have been obtained from the laboratories of H. Morkoc (University of Illinois), S. Nishino (Kyoto Institute of Technology), and V. Dmitriev (Howard University) and characterized by LTCL and FTIR reflectance. Several other researchers have agreed to provide samples in the future, including A. Khan (APA Optics), S. Nakamura (Nichia Chemical), and T. Kistenmacher (Johns Hopkins APL). With LTCL, we have not observed sharp excitonic features near the band edge of any of the samples measured to date, but do see strong deep-level luminescence in all samples, which varies significantly with growth conditions. This is illustrated by Fig. 2, which shows a composite spectrum of five AlN layers grown under different conditions by V. Dmitriev of Howard University.

FTIR reflectance data of the restrahlen bands of the nitride layers and their substrates were also obtained. By analysis of these curves, we have been able to separate the contribution of the layers from that of the substrates.

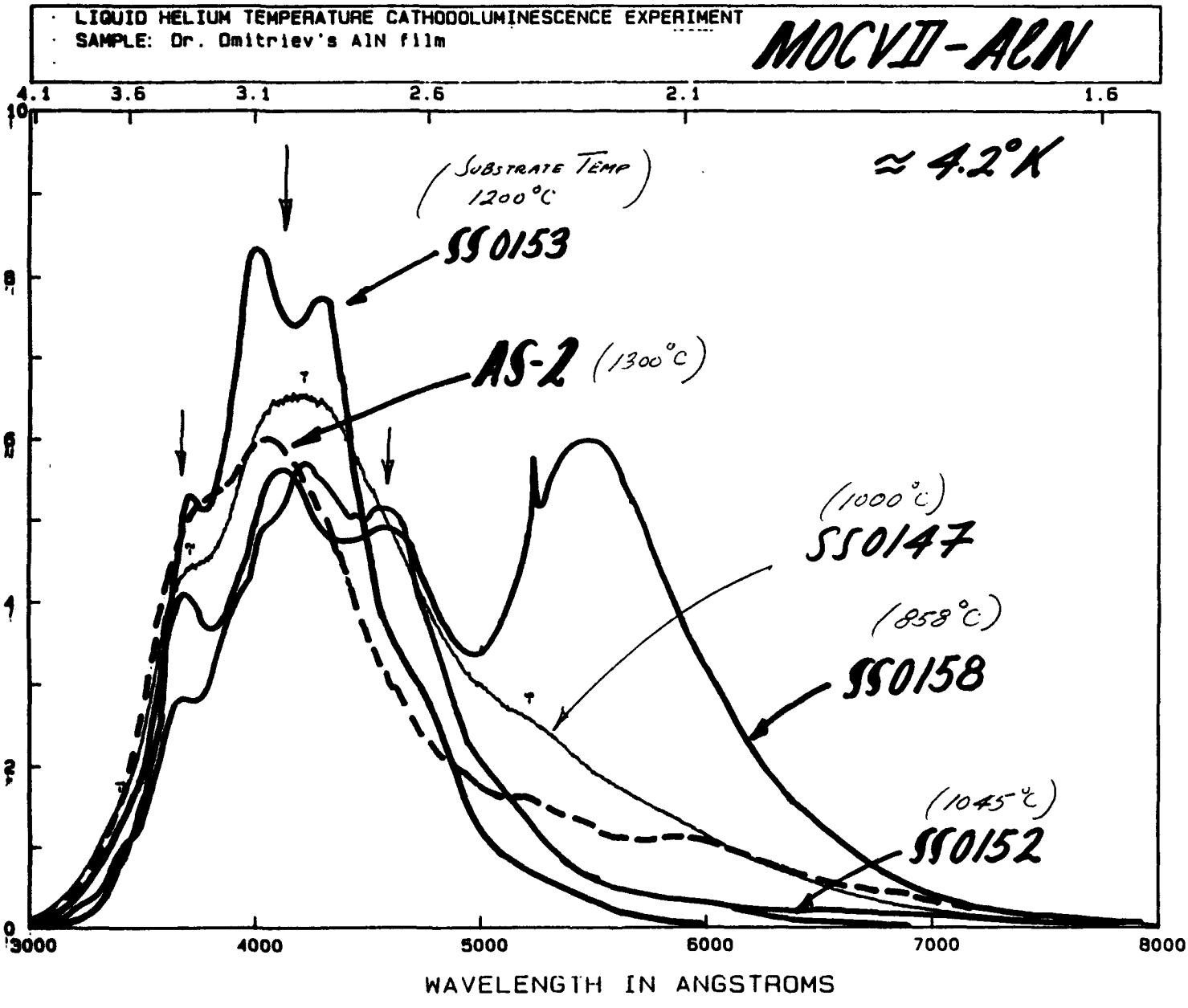

Figure 2: Spectra from 3000 to 8000Å of the low temperature cathodoluminescence (LTCL) of five aluminum nitride samples grown under different conditions by V. Dmitriev, Howard Univ.

We plan to continue to survey materials grown by different techniques and at different laboratories, to relate the quality of the layers to growth techniques. Vacuum ultraviolet reflectance spectroscopy is also planned, which will provide direct information on the band structure of these materials.

3. PROGRAM PUBLICATIONS AND INTERACTIONS

Journal Article: M. L. Colaianni, P. J. Chen, H. Gutleben, and J, T, Yates, Jr., "Vibrational Studies of CH_3I on Si(100)-(2X1): Adsorption and Decomposition of the Methyl Species", to be published in Chem. Phys. Lett.

Conference Organizing Committee and Session Organizer: W. D. Partlow, Workshop on Wide Bandgap Nitrides, St. Louis, MO, April 13, 1992.

Conference Paper: W. J. Choyke, M. F. MacMillen, and R. P. Devaty, "LTCL and FTIR Reflectivity of AlN Films on SiC and Si Substrates", Workshop on Wide Bandgap Nitrides, St. Louis, MO, April 13, 1992.

4. REFERENCES

1. M. L. Colaianni, P. J. Chen, H. Gutleben, and J, T, Yates, Jr., "Vibrational Studies of CH_3I on Si(100)-(2X1): Adsorption and Decomposition of the Methyl Species", to be published in Chem. Phys. Lett.
2. H. Gutleben, S. R. Lucas, C. C. Cheng, W. J. Choyke, and J. T. Yates, Jr., "Thermal stability of the methyl group adsorbed on Si(100): CH3I surface chemistry" Surface Science 257, 146-156 (1991).

APPENDIX I:
ADSORPTION AND DECOMPOSITION OF CH_3 ON Si(100)

Two Reprints:

1. H. Gutleben, S. R. Lucas, C. C. Cheng, W. J. Choyke, and J. T. Yates, Jr., "Thermal stability of the methyl group adsorbed on Si(100): CH_3I surface chemistry" Surface Science 257, 146-156 (1991).

2. M. L. Colaianni, P. J. Chen, H. Gutleben, and J, T, Yates, Jr., "Vibrational Studies of CH3I on Si(100)-(2X1): Adsorption and Decomposition of the Methyl Species", to be published in Chem. Phys. Lett.

Surface Science 257 (1991) 146–156
North-Holland

Thermal stability of the methyl group adsorbed on Si(100): CH_3I surface chemistry

H. Gutleben, S.R. Lucas, C.C. Cheng, W.J. Choyke [1] and J.T. Yates, Jr.
Surface Science Center, Department of Chemistry, University of Pittsburgh, Pittsburgh, PA 15260, USA

Received 28 February 1991; accepted for publication 14 May 1991

The adsorption and thermal behavior of methyl iodide on Si(100)-(2 × 1) have been studied by kinetic uptake measurements, Auger electron spectroscopy (AES) and temperature-programmed desorption (TPD) mass spectroscopy. Methyl iodide adsorbs on Si(100) at room temperature with high efficiency (initial reaction probability of unity). From the kinetic uptake measurements and the AES measurements an average saturation coverage of $(2.9 \pm 0.3) \times 10^{14}$ methyl iodide molecules/cm^2 is calculated, i.e., about one methyl iodide molecule per two silicon surface atoms. Experimental evidence is presented indicating that the molecule dissociates into a covalently bonded methyl group and an iodine atom upon adsorption. Heating causes the decomposition of the methyl group. The hydrogen atoms liberated from the methyl group mainly desorb as molecular hydrogen. The adsorbed iodine desorbs in the form of atomic iodine and possibly some small amount of hydrogen iodide as detectable by line-of-sight mass spectrometry. Less then 1% of the carbon desorbs in the form of C_2 hydrocarbon species. Neither the desorption of methane nor the desorption of methyl iodide is observed.

1. Introduction

The adsorption and thermal behaviour of organic molecules on well-defined silicon surfaces is of considerable interest since such precursors might be used in the formation of SiC or in epitaxial diamond film growth. While the adsorption and thermal behavior of unsaturated hydrocarbons on Si(100) have been studied in detail [1–8], no work has been done on the behavior of the methyl group adsorbed on Si(100). This might be due to the fact that methane does not adsorb on Si(100) [9]. In the work presented here we used methyl iodide to introduce the methyl group to the silicon surface, and have studied its thermal stability using AES and TPD mass spectroscopy.

[1] Department of Physics, University of Pittsburgh, Pittsburgh, PA 15260, USA.

2. Experimental

The experiments were carried out in a stainless steel UHV chamber pumped by a 150 ℓ/s turbo pump, a 270 ℓ/s diode ion pump and a titanium sublimation pump. The base pressure attained was 2×10^{-10} Torr. The chamber was equipped with a multicapillary array doser [10], a UTI-100C quadrupole mass spectrometer, a single-pass CMA Auger spectrometer and a tungsten spiral for the production of atomic hydrogen which was chemisorbed by line-of-sight exposure.

The doser contained a 2.2 cm diameter glass microcapillary collimator array composed of closely spaced 10 μm inside-diameter capillary cylinders of 500 μm length. The total flux out of the doser was controlled by a 3.3 μm diameter orifice seated inside the doser and by the pressure of methyl iodide stored in the gas line behind the orifice (usually about 1 Torr). The con-

Table 1
Conductance values for methyl iodide

Effusion source	Calculated CD_3I conductance (CD_3I/Torr s)
hydrogen	1.45×10^{13}
ethylene	1.43×10^{13}
acetone	1.54×10^{13}
methyl iodide	1.51×10^{13}

ductance of the orifice was calibrated by measuring the decrease of the pressure in the gas line over a period of about 8×10^4 s using a capacitance manometer. It was found that, in a first part of the calibration measurement for methyl iodide, the apparent conductance was slightly higher (about 8%) then in the rest of the measurement, possibly due to adsorption of methyl iodide on the walls of the gas line. To verify that the latter conductance value for methyl iodide was correct, calibration was done also with three other gases (hydrogen; ethylene; acetone). Assuming that the gas flow through the orifice is inversely proportional to the square root of the molecular mass the conductance values for methyl iodide as shown in table 1 were deduced:

The average value of these four measurements, i.e., $(1.48 \pm 0.05) \times 10^{13}$ CD_3I/Torr s, was used for calculating the flux of methyl iodide from the doser.

Knowing the absolute flux of methyl iodide out of the doser, the actual number of molecules striking the crystal per unit time can be calculated from the size of the microcapillary array, the size of the crystal and the distance between crystal and doser [11].

The amount of methyl iodide being adsorbed on the crystal was determined by monitoring the partial pressure of methyl iodide in the chamber during the adsorption process [12].

Using the same mass spectrometer both for the uptake measurements (random flux of gas, low partial pressure) and TPD measurements (line-of-sight, higher local partial pressure) required a special design, similar to that previously reported [12,13]. The mass spectrometer was surrounded by a stainless steel shield which contained a small axial aperture (0.47 cm diameter) on its front end. In the region around the ionizer of the mass spectrometer this cylinder was cut open (open area: 29 cm^2) to allow a high flow rate of the random gas into the mass spectrometer during the uptake measurement. The open part subtended 160° of the total circumference of the cylinder and was put in a position facing away from the gas doser so that no molecules coming out of the doser were able to strike the opening without undergoing collisions with the walls of the chamber.

During the line-of-sight TPD experiments this opening was closed by a sliding door on the cylinder. The mass spectrometer was translated [14] toward the center of the chamber by 3.8 cm when TPD experiments were performed and was translated outward to its original position for uptake measurements and when the crystal was sputtered. For TPD measurements, the distance between crystal and aperture was only about 0.2 cm. This close-coupled geometry prevented the detection of spurious desorption from the crystal holder and support leads. The sliding door was fully open when the spectrometer was pulled back for uptake measurements. To prevent vacuum welding between the stainless steel cylinder covering the mass spectrometer and the door, the latter was made of aluminum. To provide differential pumping of the mass spectrometer during the line-of-sight TPD experiments, the cylinder contained four holes (with an area 3.9 cm^2) at its end opposite from the front aperture. The line-of-sight aperture used for TPD measurements was negatively biased during the TPD experiments to prevent the possibility that electrons emitted from the ion source of the mass spectrometer would hit the crystal causing electron damage effects on the adsorbate.

The Si(100) crystals ($14.95 \times 14.95 \times 1.5$ mm; p-type, B-doped, 10 Ω cm; Czochralski grown, commercially cut and polished within 1°) were slotted on all four edges using a diamond impregnated steel string saw. They were then chemically cleaned by a peroxide/HF stripping procedure [15,16] and mounted by wedging Ta foils, which were wrapped around W support rods, into two opposite slots of the crystal [10]. A chromel/constantan thermocouple, spot-welded to a tanta-

lum foil, was spring-loaded into a third slot. The attainable crystal temperature varied from 110–1300 K. During handling and mounting of the crystal, special care was taken to prevent Ni contamination of the crystal [16]. The crystals were finally cleaned in vacuo by alternative sputtering with Ar^+ (2 kV, 2.5 μA) and heating (10 min at 970 K, 10 min at 1070 K, 10 min at 1170 K, and slowly cooling). With the exception of small traces of carbon (< 0.5 at.% within the probing depth of the AES) near the edges of the crystal the surface was free of contaminants as judged by AES. In these measurements the signal-to-noise ratio for the Si(LVV) peak was 1000.

In most of the adsorption experiments, deuterated methyl iodide (gold label 99 + % D) was used to obtain a higher desorption signal-to-background ratio for possible desorption products like deuterium and deuterated hydrocarbons. Both deuterated and non-deuterated methyl iodide were purified by numerous freeze–pump–thaw cycles. No contamination of the gases was observed with mass spectrometry.

3. Results

3.1. Adsorption

3.1.1. Kinetic uptake measurements

The adsorption experiments were performed in the following way. After the crystal had been positioned in front of the doser, a shutter was moved in between the doser and the crystal, and methyl iodide was introduced by filling the backing line with the gas. After the partial pressure of methyl iodide in the chamber had reached an almost constant value as measured by the mass spectrometer (after about 1200 s (fig. 1a)), the shutter was moved out of the beam of gas and methyl iodide was adsorbed on the crystal from the beam (fig. 1a). By moving the shutter in again, the flow of the gas onto the crystal surface was stopped. The methyl iodide flow to the doser was discontinued by pumping out the gas from the gas line.

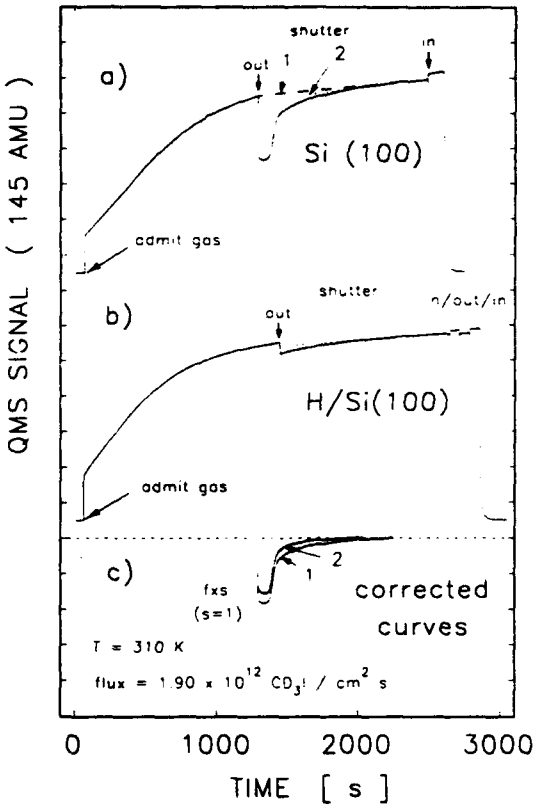

Fig. 1. (a) Kinetic uptake of CD_3I on the clean Si(100) surface using a calibrated doser. Gas flow = 1.40×10^{13} CD_3I/s; intercepted beam fraction = 0.305; crystal temperature = 310 K. (b) Same as (a) but the Si surface is saturated with hydrogen. (c) Resulting uptake curves after correction for the decreasing pumping speed of the system. Curve 1: without nonrandom-flux correction; curve 2: with nonrandom-flux correction and adsorption on sample holder subtracted.

As fig. 1 shows, there are two peculiar effects taking place during the kinetic uptake measurement:

Effect 1 – The partial pressure of methyl iodide steadily increases, especially during the first 1200 s of the experiment.

Effect 2 – Even when methyl iodide is dosed onto a Si(100) surface which has been previously saturated with monohydride (fig. 1b) (and does therefore not adsorb methyl iodide as measured by AES) there is evidence of slight uptake of methyl iodide.

We first discuss effect 1 above. The steadily increasing pressure of methyl iodide during the

experiment can be explained by a steadily decreasing pumping speed of the chamber for methyl iodide as the walls become saturated. To rule out the possibility that methyl iodide is significantly adsorbed in the doser or the microcapillary array to produce this effect, the following experiments were performed. In one experiment the shutter was removed after 130 s and the surface was exposed to methyl iodide for 60 s. In a second experiment the shutter was removed after 1200 s and methyl iodide was adsorbed for 60 s. When one considers the small amount of methyl iodide adsorbed with the shutter in place (7% of a monolayer in 1200 s, see below), both experiments resulted in exactly the same methyl iodide coverage as measured by AES. Thus the delivery of methyl iodide by the doser was constant during the 1200 s period.

When the pumping speed of the system decreases and, with a constant flux of gas into the system, the partial pressure of the gas accordingly increases (pressure × pumping speed = constant). In this case the amount of gas adsorbed by the crystal cannot be calculated simply from the area between the measured uptake curve and the line which represents the signal if no adsorption would occur (dashed line 1 in fig. 1a). The increase of the partial pressure due to random flux does not significantly increase the flux of gas onto the crystal surface because the incident flux of the dosed gas in front of the doser is much higher (~ 100 times) than the random flux of the gas in the chamber. However, the uptake experiment measures the pressure near the crystal by means of measuring the partial pressure in the chamber, and this signal measured by the mass spectrometer during the adsorption experiment is therefore inversely proportional to the pumping speed of the system. Hence a certain area increment between the dashed line 1 and the uptake curve (fig. 1a) in the early stage of adsorption (higher system pumping speed) corresponds to a greater amount adsorbed than the amount calculated from the same area increment in a later stage of the uptake experiment (lower system pumping speed).

To correct for this effect the signal measured during uptake by the mass spectrometer is divided by the corresponding value on the dashed line 1 (fig. 1a), which is a relative measure of the pumping speed of the system for methyl iodide. In this way the uptake curve is normalized to the value of the pumping speed at the beginning of the uptake measurement ("shutter out"). This normalization procedure also corrects for a day-to-day change of the sensitivity of the mass spectrometer and also for a change of the sensitivity of the mass spectrometer within one experiment, if any. This procedure is accurate as long as uptake measurements are made in time intervals where the pumping speed is changing slowly, as is the case here.

We now discuss effect 2 above. The fact that the signal measured by the mass spectrometer decreases when methyl iodide is incident on a hydrogen-passivated Si(100) surface (fig. 1b), indicates the presence of two small effects listed below:

(a) the adsorption of methyl iodide on the sample holder or on the chamber wall opposite to the doser;

(b) the flux of gas into the mass spectrometer is not totally random, i.e., when methyl iodide molecules are reflected by the shutter, a slightly larger number of molecules reaches the opening in the mass spectrometer shield than in the case the shutter is moved out of the beam.

Effect a above is indicated by the larger fractional effect seen at the beginning of the adsorption experiment than at the end (fig. 1b). Effect b above may be seen from the small fractional changes observed at the end of the experiment shown in fig. 1b when the shutter is alternately in and out.

The measured uptake curve (fig. 1a) is therefore corrected in the following way: The change in the signal when the shutter is moved in after the crystal has been exposed to methyl iodide for about 1200 s is subtracted from the signal at the beginning of the uptake ("shutter out"). The resulting point is then used to draw the dotted line (line 2 in fig. 1a) and the correction for the decreasing pumping speed is made, using this line as explained above. The same procedure is used for the experiment in which the surface has been blocked with adsorbed hydrogen, and the result-

ing spurious adsorption curve is subtracted from the uptake curve of the methyl iodide adsorption experiment (fig. 1a). Fig. 1c shows the result. Curve 1 is the uptake curve resulting after correction for the decreasing pumping speed only. Curve 2 shows the result after correction for the non-random flux effect, for the adsorption of methyl iodide on the sample holder, and for the effect of the decreasing pumping speed. Curve 2 represents our best estimate of the true uptake curve without extraneous effects. From four adsorption experiments and two experiments where the surface has been blocked with hydrogen, a coverage of $(2.8 \pm 0.1) \times 10^{14}$ CD_3I/cm^2 is calculated. The error indicates only the standard deviation of the measurements.

Shown in fig. 1c also is the mass spectrometer signal (dotted line) which is to be expected if methyl iodide adsorbs onto the Si(100) surface with an initial reaction probability, $S = 1$, given an intercepted fraction f of the gas beam = 0.305 as calculated from the size of the doser, the size of the crystal, and the distance between crystal and doser [11]. The good agreement between the dotted line position and the lowest portion of curve 2 suggests that initially $S = 1$ for CD_3I during adsorption at 310 K.

3.1.2. Corrections to the kinetic uptake measurements

The saturation coverage value calculated from the kinetic uptake measurements described above is not the true value but has to be corrected for the amount of methyl iodide adsorbed by random flux during the initial 1200 s admission period prior to opening the shutter, and for the adsorption of methyl iodide in the later stage of adsorption where the reaction probability is too small to be observed by the kinetic uptake measurement. Both corrections are done by AES. In the time (1200 s) between the introduction of methyl iodide through the doser and moving the shutter out of the beam (fig. 1a), 7% of the saturation coverage of methyl iodide is adsorbed. After the crystal has been exposed about 720 s to methyl iodide, a 6% increase to saturation coverage of the carbon and iodine AES intensity occurs from this point. Therefore the coverage value of 2.8×10^{14} CD_3I/cm^2 as calculated from the uptake area corresponds to 87% of the saturation coverage. On this basis, the saturation coverage is 3.2×10^{14} CD_3I/cm^2 or 0.94 methyl iodide molecules per 2 silicon surface atoms (a perfect Si(100) surface nominally contains 6.8×10^{14} Si atoms/cm^2).

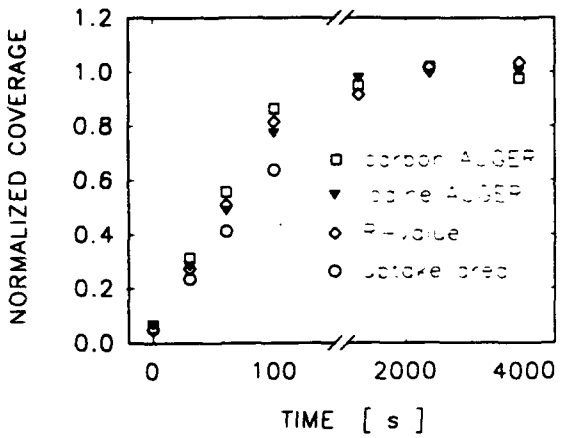

Fig. 2. Normalized coverage as a function of exposure time. Flux = 1.90×10^{12} CD_3I/cm^2s; crystal temperature = 293 K. For better comparability the R-value is represented as $(R - R_0)/(R_1 - R_0)$, as shown in section 3.1.4.

3.1.3. Comparison between the kinetic uptake measurements and the AES measurements

Fig. 2 shows the carbon and iodine AES peak-to-peak heights and the corrected uptake areas as a function of exposure time, all normalized to the respective values measured for saturation coverage. The normalization of the uptake areas includes the 13% of the saturation coverage not detected by the kinetic uptake measurement.

There are differences between the carbon and the iodine AES results, and between the AES results and the results of the kinetic uptake measurements. The latter might be in part due to the uncertainties resulting from the corrections made in the kinetic uptake measurements. Another reason may be the considerable ESD effect observed both in the carbon and iodine AES measurements. Both signals show an exponential decay with time. Assuming that the ESD cross sections are independent of coverage, all measurements were made using a standardized time

schedule instead of measuring the exponential decay of the AES signal and extrapolating to zero time. AES data were taken at least at 3 different crystal positions and averaged. The height of the Si(KLL) peak was used as reference for the sensitivity of the Auger instrument and the methyl-iodide-coverage dependent diminution of the Si(KLL) peak (7.5% for saturation coverage) was included in the normalization procedure.

Using the result of the kinetic uptake measurement which shows that the initial sticking coefficient for the adsorption of methyl iodide on Si(100) at 310 K is unity (fig. 1c), the saturation coverage can be calculated from the AES data. From an extrapolation of the initial linear increase of the Auger peak height with exposure to the saturation values of the carbon and iodine AES intensities, a saturation value of 2.6×10^{14} CD_3I/cm^2 is calculated. We take the average result of both measurement methods as saturation coverage of methyl iodide on Si(100), i.e.,$(2.9 \pm 0.3) \times 10^{14}$ CD_3I/cm^2 or 0.85 ± 0.1 methyl iodide molecules per 2 silicon surface atoms.

3.1.4. *Influence of the adsorbed methyl iodide on the Si(LVV) auger peak shape*

As can be seen in fig. 3 the adsorption of methyl iodide drastically reduces the peak height of the Si(LVV) AES peak. In addition, a change in the Auger peak shape is observed which can be expressed by the parameter $R = A/B$ as defined in fig. 3a. It is found that the value of R is strictly proportional to the methyl iodide coverage θ, where θ is the mean relative coverage based on the average of the carbon and iodine AES measurement,

$$R = R_0 + (R_1 - R_0)\theta,$$

where R_0 is the R-value of the clean surface, and R_1 is the R-value when the surface is saturated with methyl iodide. A linear fit to the data gives $R_0 = 0.143$ and $R_1 = 0.307$.

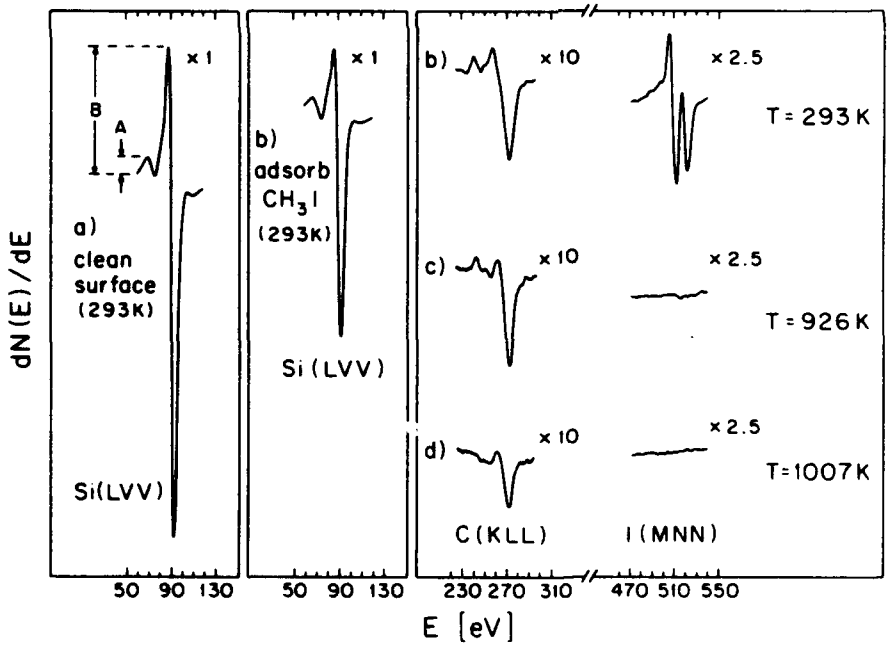

Fig. 3. Auger spectra for methyl iodide adsorption and decomposition. (a) Si(LVV), clean surface; (b) Si(LVV), C(KLL) and I(MNN) after adsorption of methyl iodide at 293 K; $\theta = 0.95$; (c) after heating to 926 K; (d) after heating to 1007 K. Primary beam energy = 3 kV; beam current = 3 μA.

3.2. Thermal effects on adsorbed layer

3.2.1. Auger measurements

Fig. 4 shows the carbon and iodine AES intensity, θ, measured after an almost saturated adlayer had been heated to different temperatures. In these measurements, it is almost certain that the electron beam causes severe chemical damage of the surface species, but this has been shown to be of secondary importance to the C(KLL) or I(MNN) Auger intensity. The Auger electron beam influences only a small fraction of the adsorbate, and the beam is moved to a new position for each point shown in fig. 4. Also shown is the R-value as a function of temperature. The iodine signal begins to decrease at about 700 K and becomes zero above approximately 900 K (fig. 4a). The carbon AES signal decreases in a different fashion and is still about 90% of its initial value at a point where no iodine is detectable any more (fig. 4b). At the same time

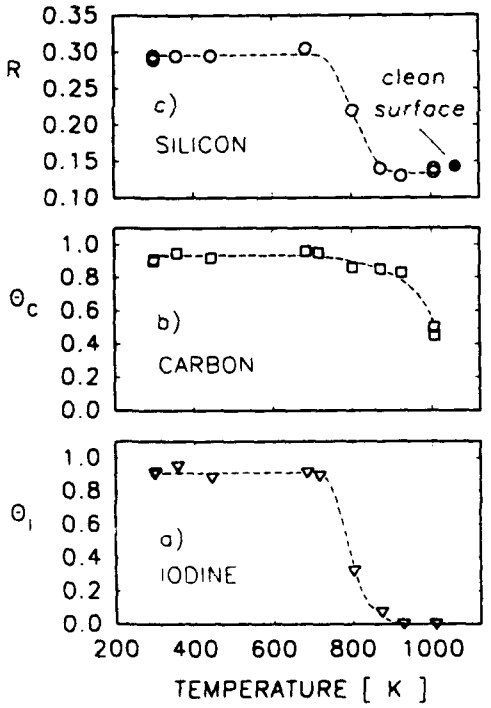

Fig. 4. Thermal effects on adsorbed methyl iodide using AES. The Auger intensities are normalized to the intensities of the saturated adlayer. The full circle in panel (c) shows the R-value of the clean surface.

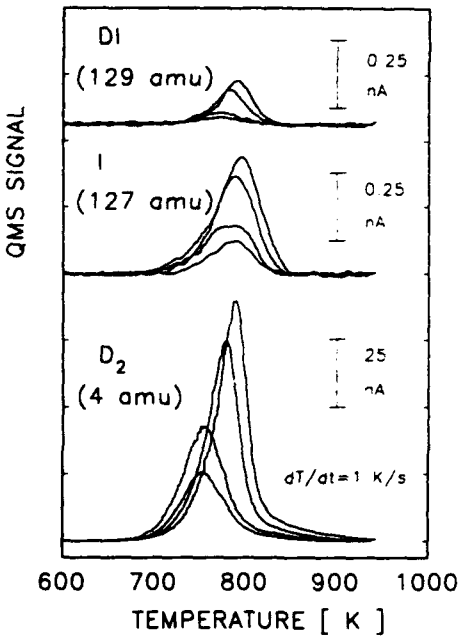

Fig. 5. Temperature-programmed desorption from CD_3I layer on Si(100). The four curves correspond to an initial CD_3I coverage, $\theta = 0.30, 0.52, 0.82$ and 1.00; heating rate a 1 K/s.

a change in the carbon Auger lineshape is observed as shown in fig. 3. Heating to still higher temperature decreases the carbon AES signal further. Simultaneously the R-value decreases and finally reaches the value of the clean surface after all the iodine has disappeared (fig. 4c).

3.2.2. TPD-mass spectra

Fig. 5 shows TPD spectra for different masses obtained after different exposures of methyl iodide. The main mass signals observed are 4 amu (D_2), 127 amu (I) and 129 amu (DI). Beside these masses there are also some small desorption peaks of masses 26, 28, 30 and 32 amu (after CD_3I has been adsorbed) and mass 24, 25, 26, 27 and 28 amu (after CH_3I has been adsorbed) detected, occurring at about the same temperature as the main desorption peaks shown in fig. 5. The 32 amu feature for CD_3I may be due to C_2D_4 desorption; the 28 amu feature for CH_3I may be due to C_2H_4 desorption. Comparing the areas of these peaks with the measured mass spectrometer fragmentation pattern of ethylene shows that

the observed C_2 hydrocarbon species cannot be solely attributed to desorption of ethylene.

Since ethylene adsorbs and desorbs with little dissociation on Si(100) [1,2,8], a calibration experiment was performed with ethylene. From a comparison between the areas of the desorption peaks it is estimated that less than 1% of the carbon in a saturated methyl iodide adlayer desorbs as C_2H_4 and as other hydrocarbon species. To verify that these small desorption features were not caused by desorption from the sample holder, the Si(100) surface was blocked with chemisorbed atomic hydrogen and then exposed to methyl iodide. No desorption of C_2 hydrocarbon species was found.

A search for further desorption products like methane, ethane, higher hydrocarbons, silicon monoiodide, molecular iodine and methyl iodide yielded negative results.

To calibrate the absolute amount of molecular hydrogen produced by decomposition of the methyl iodide adlayer at full coverage, we adsorbed atomic hydrogen on the Si(100) surface. The atomic hydrogen was produced from molecular hydrogen by means of a tungsten spiral heated to about 1800 K. If the temperature of the crystal was 630 K during hydrogen exposure, only the silicon monohydride, H(a),was formed. At a crystal temperature of 400 K both monohydride and dihydride were formed [17]. Both cases gave essentially the same desorption peak areas for the saturated monohydride adlayer on Si(100) (fig. 6). Figure 6 also shows the hydrogen desorption peak area after CH_3I had been adsorbed ($\theta = 0.96$). Taking the mean of the two experiments and extrapolating to $\theta = 1$ shows that the amount of hydrogen desorbing from the saturated methyl iodide adlayer corresponds to 97% of the amount of hydrogen desorbing from the saturated monohydride phase.

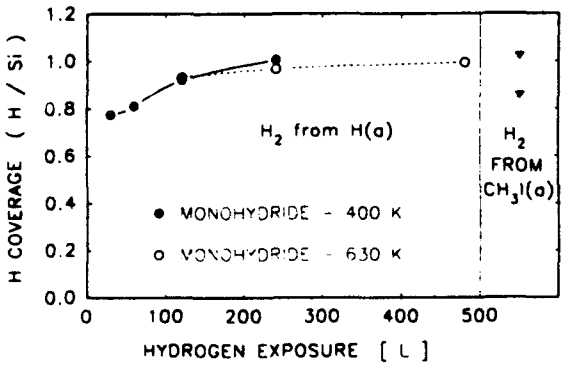

Fig. 6. Comparison of hydrogen yields from H(a) and $CH_3I(a)$. The hydrogen exposures are given in Langmuir units of molecular hydrogen (not corrected for ion gauge sensitivity). The methyl iodide coverage was $\theta = 0.96$ in both experiments.

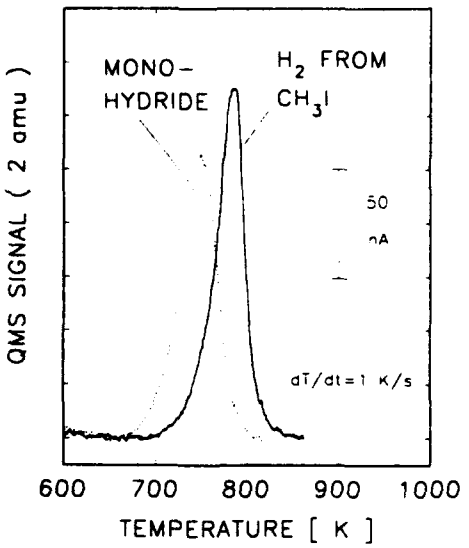

Fig. 7. Hydrogen desorption from the saturated monohydride phase (adsorbed at 630 K) and from adsorbed CH_3I ($\theta = 0.96$); heating rate = 1 K/s.

Fig. 7 shows the hydrogen desorption peaks resulting from the saturated monohydride phase and from adsorbed methyl iodide ($\theta = 0.96$). Hydrogen produced from the methyl iodide adlayer desorbs at a temperature about 30 K higher than the monohydride phase.

4. Discussion

4.1. Adsorption of methyl iodide

Methyl iodide adsorbs on Si(100) with an initial reaction probability of $S = 1$ at 310 K (fig. 1c). The reaction probability remains constant up to about 70% of the saturation coverage (fig. 2), Indicating that adsorption involves a precursor mechanism [18]. The experimental results listed

below indicate that methyl iodide undergoes dissociation upon adsorption on Si(100).

(1) A characteristic, strictly coverage-dependent change of the line shape of the Si(LVV) Auger peak is found (figs. 2 and 3). This must be due to covalent bonding to Si of species resulting from methyl iodide dissociation on the surface. Madden [19] reports a similar change of the Si(LVV) AES lineshape when atomic hydrogen is adsorbed on Si(100). From the AES (as well as characteristic loss spectroscopy experiments), Madden concludes that the density of states of both the valence band and the conduction band of Si(100) is changed by the covalent bonding of atomic hydrogen to Si.

(2) No thermal desorption of methyl iodine is found.

(3) According to the kinetic uptake measurements and the AES measurements, the saturation coverage of methyl iodide on Si(100) is $(2.9 \pm 0.3) \times 10^{14}$ methyl iodide molecules/cm^2. The unreconstructed Si(100) surface nominally contains 6.8×10^{14} Si atoms/cm^2. On the Si(100)-(2 × 1) surface, Si dimers form across the surface so that one dangling bond is left on every silicon atom [20]. According to recent STM [20–22] and X-ray diffraction [23] experiments as well as theoretical work [24,25] these dimers are unsymmetrical, rapidly converting between two possible configurations. For silicon dimers near surface defects, this configurational conversion seems to be frozen [20–22]. The number of defect sites (e.g., missing dimers, steps and contamination sites) depends on the conditions used for surface preparation [20,26]. Typical values of the defect density reported are between 5 and 10% [20,21]. Hence the saturation coverage of 2.9×10^{14} methyl iodide molecules/cm^2 agrees well with the value expected from dissociative adsorption of methyl iodide, i.e., the methyl group and the iodine atom bond to one dangling bond each, as shown schematically in fig. 8.

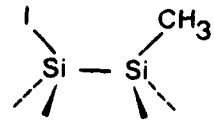

Fig. 8. Model for adsorbed CH_3I layer on Si(100)-(2 × 1).

4.2. Desorption

Thermal desorption experiments show that CD_3I yields D_2, I and DI (fig. 5).

The mass spectrometer fragmentation pattern of DI or HI is unavailable in the literature, and was therefore measured, giving $HI^+/I^+ = 1.7$ for 70 eV electrons [27]. Thus using this cracking pattern, the relative yield of $DI^+/I^+ \approx 0.33$ (fig. 5) or $HI^+/I^+ \approx 0.34$ in thermal desorption suggests that the production of I by thermal desorption greatly exceeds the production of DI. The possibility of small amounts of DI formation inside the mass spectrometer ion source cannot be excluded.

On the other hand, we have evidence that hydrogen atoms, produced on the surface by decomposition of the methyl group, might be able to combine with the adsorbed iodine atoms to form hydrogen iodide. In experiments where a saturated methyl iodide adlayer was exposed to atomic hydrogen at room temperature, It was found that atomic hydrogen removes the iodine with high efficiency [28], probably by an Eley–Rideal type mechanism as postulated for the reaction of atomic hydrogen with deuterium adsorbed on Si(100) [29].

Since the desorption of HI and C_2 hydrocarbons are minor products compared to the desorption of iodine atoms, the amount of hydrogen desorbing from the saturated methyl iodide layer should correspond to almost $3 \times 2.9 \times 10^{14}$ H/cm^2 = 8.7×10^{14} H/cm^2 since each CH_3 group contributes 3 hydrogen atoms. Calibration of the H_2 desorption peak area from methyl iodide with the amount of H_2 desorbing from the saturated monohydride phase (6.8×10^{14} H/cm^2) (fig. 6), gives 6.6×10^{14} H/cm^2 desorbing from the saturated methyl iodide layer. It is unclear whether this discrepancy of ~25% simply reflects the combined uncertainties in the coverage measurements and the hydrogen calibration, respectively, or is caused by a physical phenomenon like diffusion of hydrogen into the silicon bulk.

Table 2
Desorption/decomposition behavior of organic molecules adsorbed on Si(100)

Molecule adsorbed		Percentage carbon desorbing	Carbon-containing desorption products	TPD-peak maximum (T_p (H_2)) (K)
methyl iodide	[this work]	< 1	C_2H_x; $x \leq 4$	790
acetylene	[7]	5	C_2H_2	780
ethylene	[2,8]	95	C_2H_4	785
propylene	[5]	35	C_3H_6	[a]

[a] Only heated to 630 K.

Carbon AES measurements, after heating the adlayer to different temperatures (fig. 4), show a decrease of the carbon AES signal above ~ 750 K. This effect is caused by carbon diffusion into the bulk. Heating above 800 K increases the extent of this carbon diffusion process dramatically, as has been observed on Si(100) using other hydrocarbon adsorbates [6,7].

Table 2 compares desorption/decomposition behavior of several unsaturated hydrocarbons adsorbed on Si(100) with the behavior of the methyl group. It may be seen that adsorbed CH_3I is an efficient source of surface carbon compared to some other adsorbed hydrocarbons. In addition, the hydrogen liberated by thermal decomposition of the adsorbed hydrocarbons desorbs in all cases at about the same temperature (780–790 K), a temperature which is about 20 to 30 K higher than the desorption temperature of the hydrogen of the monohydride phase.

5. Summary

(1) Methyl iodide adsorbs on Si(100) at 310 K with high efficiency (initial reaction probability of unity). From kinetic uptake measurements and AES measurements an average saturation coverage of $(2.9 \pm 0.3) \times 10^{14}$ methyl iodide/cm^2 is calculated. Within experimental error this value corresponds to one methyl iodide molecule per two silicon surface atoms.

(2) Adsorption leads to dissociation of the methyl iodide molecule resulting in covalent bonding of the methyl group and the iodine atom to the silicon substrate.

(3) It is proposed that heating causes the thermal decomposition of the chemisorbed methyl group. The hydrogen atoms liberated from the methyl group desorb mainly as molecular hydrogen, beginning near 700 K. The adsorbed iodine desorbs mainly in the form of iodine atoms and possibly some small amount of hydrogen iodide.

(4) Less than 1% of the carbon desorbs as C_2 hydrocarbon species. The carbon remaining on the surface starts to diffuse into the bulk at 750 K. No desorption of methane or methyl iodide is found.

Acknowledgements

We would like to thank Dr. P.A. Taylor and Dr. R.M. Wallace for valuable discussions. Financial support was provided by the Air Force Office of Scientific Research (AFOSR) Contract No. F4962084C-0063, in a subcontract from Westinghouse Science and Technology Center, and by the Fonds zur Forderung der Wissenschaftlichen Forschung, Austria.

References

[1] C.C. Cheng, R.M. Wallace, P.A. Taylor, W.J. Choyke and J.T. Yates, Jr., J. Appl. Phys. 67 (1990) 3693.
[2] C.C. Cheng, W.J. Choyke and J.T. Yates, Jr., Surf. Sci. 231 (1990) 289.
[3] J. Yoshinobu, H. Tsuda, M. Onchi and M. Nishijima, J. Chem. Phys. 87 (1987) 7332.
[4] M. Nishijima, J. Yoshinobu, H. Tsuda and M. Onchi, Surf. Sci. 192 (1987) 383.

[5] M.J. Bozack, W.J. Choyke, L. Muehlhoff and J.T. Yates, Jr., J. Appl. Phys. 60 (1986) 3750.
[6] M.J. Bozack, P.A. Taylor, W.J. Choyke and J.T. Yates, Jr., Surf. Sci. 179 (1987) 132.
[7] P.A. Taylor, R.M. Wallace, C.C. Cheng, W.H. Weinberg, M.J. Dresser, W.J. Choyke and J.T. Yates, Jr., J. Chem. Phys., submitted.
[8] L. Clemen, R.M. Wallace, P.A. Taylor, M.J. Dresser, W.J. Choyke, W.H. Weinberg and J.T. Yates, Jr., J. Chem. Phys., submitted.
[9] M.J. Bozack, P.A. Taylor, W.J. Choyke and J.T. Yates, Jr., Surf. Sci. 177 (1986) L933.
[10] M.J. Bozack, L. Muehlhoff, J.N. Russel, Jr., W.J. Choyke and J.T. Yates, Jr., J. Vac. Sci. Technol. A 5 (1987) 1.
[11] A. Winkler and J.T. Yates, Jr., J. Vac. Sci. Technol. A 6 (1988) 2929;
C.T. Campbell and S.M. Valone, J. Yac. Sci. Technol. A 3 (1985) 408.
[12] V.S. Smentkowski and J.T. Yates, Jr., J. Vac. Sci. Technol. A 7 (1989) 3325.
[13] R.M. Wallace, P.A. Taylor, W.J. Choyke and J.T. Yates, Jr., J. Appl. Phys. 68 (1990) 3669.
[14] H. Gutleben and J.T. Yates, Jr., J. Vac. Sci. Technol. A 9 (1991) 170.
[15] W. Kern, RCA Engineer 28. 4 (1983) 99; Semicond. Int. April (1984) 94.
[16] R.M. Wallace, C.C. Cheng, P.A. Taylor, W.J. Choyke and J.T. Yates, Jr., Appl. Surf. Sci. 45 (1990) 201.
[17] C.C. Cheng and J.T. Yates, Jr., Phys. Rev. B 43 (1991) 4041.
[18] W.H. Weinberg, in: Kinetics of Interface Reactions, Eds. M. Grunze and H.J. Kreuzer (Springer, New York, 1987) p. 94.
[19] H.H. Madden, Surf. Sci. 105 (1981) 129.
[20] R.J. Hamers, R.M. Tromp and J.E. Demuth, Phys. Rev. B 34 (1986) 5343.
[21] R.J. Hamers and U.K. Kohler, J. Vac. Sci. Technol. A 7 (1989) 2854.
[22] R. Wiesendanger, D. Burgler, G. Tarrach and H.-J. Guntherrodt, Surf. Sci. 232 (1990) 1.
[23] N. Jedrecy, M. Sauvage-Simkin, R. Pinchaux, J. Massies, N. Greiser and V.H. Etgens, Surf. Sci. 230 (1990) 197.
[24] P.C. Weakliem, G.W. Smith and E.A. Carter, Surf. Sci. Lett. 232 (1990) L219.
[25] N. Roberts and R.J. Needs, Surf. Sci. 236 (1990) 112.
[26] D. Dijkkamp, E.J. van Loenen, A.J. Hoeven and J. Dieleman, J. Vac. Sci. Technol. A 8 (1990) 218.
[27] We thank Mr. J.V. Johnson and Mr. N.A. Yates for making this measurement at the University of Florida, using a quadrupole mass spectrometer. A comparison of the HI mass spectrum with that of other hydrogen halides is given below and substantiates the correctness of the measured HI cracking pattern: HCl: $HCl^+/Cl^+ = 5.9$ [30]; HBr: $HBr^+/Br^+ = 2.2$ [31]; HI: $HI^+/I^+ = 1.7$ [this work].
[28] To be published.
[29] K. Sinniah, M.G. Sherman, L.B. Lewis, W.H. Weinberg, J.T. Yates, Jr. and K.C. Janda, J. Chem. Phys. 92 (1990) 5700.
[30] E. Stenhagen, S. Abrahamsson and F.W. Mc Lafferty, Eds., Atlas of Mass Spectral Data, Vol. 1 (Interscience, New York, 1969) p. 8.
[31] E. Stenhagen, S. Abrahamsson and F.W. Mc Lafferty, Eds., Atlas of Mass Spectral Data, Vol. I (Interscience, New York, 1969) p. 104.

Submitted to: Chem. Phys. Lett.

*Date: 27 January 1992

Vibrational Studies of CH_3I on Si(100)-(2x1): Adsorption and Decomposition of the Methyl Species

M.L. Colaianni, P.J. Chen,‡ H. Gutleben‡‡ and J.T. Yates, Jr.

Surface Science Center
Department of Chemistry
University of Pittsburgh
Pittsburgh, PA 15260

‡Department of Physics, University of Pittsburgh, Pittsburgh PA 15260

‡‡Present address: Lenzing AG, A-4800 Lenzing, Austria

Vibrational Studies of CH_3I on Si(100)-(2x1): Adsorption and Decomposition of the Methyl Species

M.L. Colaianni, P.J. Chen, H. Gutleben and J.T. Yates, Jr.

Surface Science Center
Department of Chemistry
University of Pittsburgh
Pittsburgh, PA 15260

Abstract

The dissociative adsorption of CH_3I to adsorbed CH_3 and I on a clean Si(100)-(2x1) surface has been studied by high resolution electron energy loss spectroscopy (HREELS), temperature programmed desorption (TPD) and Auger electron spectroscopy (AES). The thermal stability of CH_3(a) to 600 K has been witnessed spectroscopically. At higher temperatures, CH_3(a) decomposes to CH(a), possibly via the production of intermediate $=CH_2$(a) species. The CH(a) species is stable to ~800 K. HREELS and TPD show that following CH_3I dissociative adsorption at 100 K, a multilayer of undissociated CH_3I is condensed on the substrate. Upon heating, this condensed overlayer is desorbed with a peak temperature of 225 K. H_2 and I desorption occur near 785 K, leaving adsorbed carbon on the Si(100) surface.

I. Introduction

The formation and stability of methyl groups on metal surfaces has been the subject of much scientific interest. This interest has lead to the development of a variety of techniques to prepare methyl species on these surfaces. These techniques include the molecular beam activation of methane [1-4], the photodissociation of adsorbed methyl halides [5-8] and the thermal decomposition of $-CH_3$ containing molecules, such as CH_3I on Al(111) [9] and Pt(111) [10]. In addition, recent work has involved the direct adsorption of CH_3 radicals from a beam [11].

Despite the body of knowledge concerning the behavior of $-CH_3$ on metal surfaces, the formation and thermal stability of $-CH_3$ on silicon is relatively unexplored. Only two recent studies have identified a $-CH_3$ adsorbate on the Si(100)-(2x1) surface [12,13]. A room temperature kinetic uptake study measured the full-coverage adsorption of one CH_3I molecule per Si dimer site, and, based on Auger lineshape changes, assigned the adsorbed species to CH_3(a) and I(a) [12]. Adsorbed CH_3(a) groups were postulated to decompose below the onset of H_2 desorption (700 K) [12]. Another study utilized TPD and HREELS to examine the behavior of $Zn(CH_3)_2$ on Si(100)-(2x1) [13]. A molecularly adsorbed $Zn(CH_3)_2$ species was observed at 90 K. Heating above 350 K caused desorption of molecular $Zn(CH_3)_2$ and also eliminated the Zn-C vibrational mode, while the CH_x modes in the spectrum persisted, suggesting that $-CH_3$ species were stabilized on Si(100). The absence of a characteristic Si-H stretching mode at 350 K also signified the presence of an adsorbed $-CH_3$ species. Heating above 575 K resulted in the appearance of a Si-H stretching band as adsorbed CH_3 species decomposed; however, the lack of any changes in the observed C-H modes (i.e., shifts in the C-H stretching frequencies or changes in the CH_3 rocking or

deformation modes) led the authors to conclude that the -CH_3 was decomposing directly to adsorbed -C and -H [13].

Other studies have not observed a -CH_3 adsorbate on silicon. Methyl chloride was found to dissociate on an alkali-covered Si(100)-(2x1) [14], though the lack of an carbon Auger signal lead the authors to propose that the CH_3(a) moieties desorbed as ethane upon decomposition of CH_3Cl. In another study the decomposition of trimethylgallium onto Si(100)-(2x1) was examined by HREELS [15]. This molecule, however, was found to decompose largely via an intramolecular process, liberating CH_4, without involving any Si-CH_3 chemistry.

In this study we report the direct observation of CH_3(a) decomposing to CH_x(a) on the Si(100)-(2x1) surface. In addition, we follow the thermal desorption products from CH_3I/Si(100)-(2x1) up to 1000 K. We show that CH_3I is dissociatively adsorbed by the Si(100)-(2x1) surface, even at temperatures as low as 100 K, and that only above 600 K do the CH_3(a) species on Si(100) begin to decompose.

II. Experimental

The experiments were performed in two separate stainless steel UHV systems. The vibrational and Auger spectra were taken in a chamber equipped with a Leybold-Heraeus ELS-22 high resolution electron energy loss spectrometer (HREELS), a Perkin-Elmer single pass Auger electron spectrometer (AES) and a low energy electron diffraction (LEED) apparatus. A detailed description of this chamber has been published previously [16]. The base pressure was always below 1×10^{-10} mbar. While dosing CH_3I and during the experimental measurements, a liquid-nitrogen cooled stainless steel cold finger was used to keep the pressure below 7×10^{-11} mbar.

The HREEL spectrometer utilized a primary beam energy of 4.2 eV with a full

width at half maximum (FWHM) of 65 - 70 cm^{-1}. Approximately 1 x 10^5 and 2 x 10^5 counts per second (cps) were obtained in the elastic beam off the clean and the CH_3I-dosed Si(100) surface, respectively. The spectra were recorded digitally and processed in a manner previously described [17]. The AES was operated with a primary beam of 3 keV using 3 μA emission measured at the crystal. A 3.5 V (peak-to-peak) modulation voltage was applied to the analyzer.

The second UHV chamber housed an identical Auger spectrometer and a UTI 100C mass analyzer. All temperature programmed desorption (TPD) measurements were performed in this chamber which achieved a typical base pressure of 2 x 10^{-10} mbar. The mass spectrometer was surrounded by a stainless-steel shield containing a 4.7 mm axial aperture for line-of-sight desorption studies. Temperature programming (1 - 2 K/s) was accomplished by use of a 10 A power supply under the control of a Honeywell Universal Digital Controller (Model 5000). The TPD spectra were recorded digitally using a Tecknivent multiplexer.

Preparation of the B-doped 6 ohm-cm Si(100) single crystals (13 mm x 13 mm x 1.5 mm) was identical for both chambers and these procedures have already been described in detail [18]. Great care was taken to ensure that the crystal did not become contaminated by Ni, either by its initial preparation for mounting (involving the cutting of slots in the sides of the crystal by a diamond-impregnated stainless steel string saw blade) or by direct contact with our Ni-containing chromel-constantan thermocouple wire. A tantalum foil envelope was used to encase the thermocouple wires prior to insertion into a slot in the crystal to prevent contact with the silicon crystal [18]. A chemical stripping and oxidation procedure utilizing hydrogen peroxide replaced the contaminated oxide layer with a clean oxide layer [19]. Once in vacuum the crystals were cleaned by Ar^+ sputtering (2.0 - 2.5 keV) and annealed to 1200 K to regenerate an ordered (2x1) surface. For a detailed description of the

crystal mounting the interested reader is referred to ref. 20.

The CH_3I and CD_3I gases employed in this study were purchased from Chemalog and Aldrich Chemical Co., respectively. Their purification and quantitative transfer to glass containers has been described in detail previously [9]. The gases were introduced into the chambers through calibrated effusive beam dosers [20] which allow the surface to be reproducibly exposed to controlled quantities of gases while keeping the background pressure below 2×10^{-10} mbar.

III. Results and Discussion

A. Vibrational Studies of CH_3I Adsorption

Figures 1A(a) and 1B(a) show the vibrational spectra of submonolayer and multilayer exposures of CH_3I on a Si(100)-(2x1) surface at 100 K, respectively. Loss features at 525, 900 and 1250 cm^{-1} are the most intense modes observed after multilayer exposures. These spectral features are easily assignable to molecular CH_3I modes [21]; the ν(C-I) at 533 cm^{-1}, the $\rho(CH_3)$ at 882 cm^{-1} and the intense $\delta_s(CH_3)$ mode at 1252 cm^{-1} are reported for $CH_3I(g)$ [21]. The presence of the C-I stretching mode at 525 cm^{-1}, and the absence of any Si-H stretching features near 2100 cm^{-1}, clearly indicate the presence of a molecularly adsorbed CH_3I overlayer at higher exposures. In addition, both $\nu_{as}(CH_3) = 3080$ cm^{-1} and $\nu_s(CH_3) = 3000$ cm^{-1} are poorly resolved.

The 525 cm^{-1} ν(C-I) mode observed at high exposures is absent on the low exposure spectrum [Fig. 1A(a)], indicating that at submonolayer exposures the C-I bond is dissociated upon adsorption. The presence of the C-H stretching mode between 2900 - 3050 cm^{-1} [22,23], and the absence of a Si-H stretching mode near 2100 cm^{-1} [24] reveals further that the adsorbed $-CH_3$ moiety remains intact on the Si(100)-(2x1) surface at 100 - 200 K.

The dissociatively adsorbed iodine which bonds to the Si(100) surface is believed to produce the loss observed at 435 cm^{-1} for submonolayer exposures, Figs. 1A(a and b). Though this frequency is slightly higher than the 365 cm^{-1} Si-I frequency reported by Bellamy [23], neither C-H, Si-H nor Si-C vibrational modes have been reported in this spectral region. We therefore assign the 435 cm^{-1} mode to the Si-I stretching vibration.

HREEL spectra recorded after heating multilayer coverages of CH_3I on Si(100) to 200 K for one minute support our assignment of a molecular CH_3I overlayer condensed over a dissociated Si-CH_3 and Si-I layer. The vibrational spectrum of the CH_3I multilayer undergoes a complete conversion upon heating to 200 K [Figs. 1B(a-b)], becoming very similar to the low coverage dissociatively adsorbed Si-CH_3 and Si-I layer [Compare Figs. 1A(a and b) to 1B(b)]. After heating the CH_3I multilayer to 200 K, vibrational modes are observed at 435, 710, 1260, 1425, 1550 cm^{-1} and near 3000 cm^{-1}. All of these modes are easily related to the adsorbed Si-I mode (435 cm^{-1}) or to CH_3 modes. For brevity, most of the assignments will not be written here but are provided in Fig. 1 and in Table I. To prevent confusion it should be mentioned that two CH_3 rocking modes are assigned in these spectra, a $\rho(CH_3)$ at 710 cm^{-1} which we assign to Si-CH_3, and a $\rho(CH_3)$ at 900 cm^{-1} originating from molecular CH_3I [21].

Therefore, vibrational spectra of CH_3I adsorbed on Si(100)-(2x1) reveal that at 100 K, CH_3I is dissociatively adsorbed as -CH_3 and -I. This is in agreement with the previous results from a CH_3I/Si(100)-(2x1) study performed at 300 K which did not involve vibrational spectroscopy [12]. Higher exposures at 100 K produce a molecularly adsorbed CH_3I overlayer.

To distinguish between desorption and decomposition of the molecularly adsorbed overlayer upon heating to 200 K, a TPD study of a multilayer coverage of CD_3I is shown in Fig 2. Figures 2(a-c) show the detection of I^+, CD_3I^+ and

D_2^+ mass spectrometer species from the Si(100)-(2x1) surface during TPD after a large exposure of ~2.4 x 10^{15} CD_3I/cm^2 at 130 K. I^+ originates from atomic I desorption and from the small amount of DI detected [12]. A search for I_2 thermal desorption was unsuccesful. Here we will only consider the desorption of molecular CD_3I^+ [Fig. 2(b)]. This spectrum shows the desorption of a weakly-adsorbed CD_3I species (T_{peak} = 195 K) which precedes a broad CD_3I desorption process extending to ~500 K. Some of this desorption may occur from the support assembly for the Si(100) crystal. The narrow low-temperature desorption peak confirms that the multilayer $CH(D)_3I$ species, observed by HREELS after high exposures, desorbs from the overlayer by heating to 200 K for one minute, as was observed in Fig. 1.

B. Thermal Decomposition of the $-CH_3$ Species.

Vibrational spectra [Fig. 3] show that heating the adsorbed $-CH_3$ species causes its decomposition to CH_x (x=1 or 2) species. Characteristic C-H_x ($3 \geq x \geq 1$) vibrational modes are observed in three spectral regions: the C-H stretching modes in the 2800 - 3200 cm^{-1} region, and C-H deformation modes in the 1100 - 1600 and 700 - 1000 cm^{-1} regions [22,23]. The vibrational spectrum shown in Fig. 3(a) was obtained after CH_3I adsorption onto Si(100)-(2x1) at 300 K. An identical spectrum is obtained by dosing CH_3I at 100 K followed by heating to 300 K. No changes in the vibrational spectra were observed at any temperatures up to 600 K (spectra not shown). At 600 K [Fig. 3(b)] a very weak vibrational loss at 2140 cm^{-1}, corresponding to a Si-H stretching mode, begins to appear. Further heating to 700 K [Fig. 3(c)] causes three pronounced changes as shown in the vibrational spectrum. These are: (1) a large intensification of the Si-H mode at 2140 cm^{-1}; (2) an apparent shift of the $\nu(CH_3)$ peak at 2990 cm^{-1} to 2920 cm^{-1}; and (3) a new frequency mode developing at 980 cm^{-1}.

Extensive vibrational studies of hydrogen adsorption onto Si have established that the Si-H stretching mode appears near 2140 cm^{-1} [24]. The Si-H loss observed in this study at 700 K suggests that the adsorbed $-CH_3$ species have begun to decompose to CH_2(a) and/or CH(a) species. Unfortunately, attempting to resolve all three of the possible species on the surface, $-CH_3$, $=CH_2$ and CH, using vibrational data alone is difficult, since frequencies in the 1100 - 1600 cm^{-1} region can be assigned to either CH_3 or CH_2 vibrational modes [15,22,23], and the new peak which develops at 980 cm^{-1} can be assigned to either a CH_2 rocking mode [22] or to a C-H deformation mode [15,23].

To better understand the vibrational losses which are observed, we will refocus our discussion onto our assignment of the CH species. The vibrational bands of this species are resolvable after heating to 775 K. The vibrational spectrum recorded after heating to 775 K [Fig. 3(d)] shows that all the CH_3 and CH_2 deformation modes in the 1100 - 1600 cm^{-1} region have been removed, indicating the decomposition of all the CH_3 and CH_2 species. However, it also shows that an attenuated C-H stretching mode is still observed at 2970 cm^{-1} [Fig. 3(d)]. This strongly suggests that only the CH species remains on the surface after heating to 775 K. With the removal of the overlapping vibrational modes related to CH_3 and CH_2 species (1100 - 1600 cm^{-1}), we can now assign the 945 cm^{-1} peak observed after heating to 775 K to the δ(C-H) bending deformation.

The HREEL spectra recorded after heating to 300 and 775 K [Figs. 3(a) and 3(d)] show the characteristic vibrational features from adsorbed $-CH_3$ and CH species, respectively. Comparing these observed $-CH_3$ and CH frequencies to the spectra recorded after heating to 600 and 700 K reveals that all the CH_x vibrational losses observed at these temperatures can be explained as resulting from a mixture of CH_3 and CH species on the surface. In other words, a characteristic CH_2 vibrational band below 1600 cm^{-1} is not resolvable in spectra

3(b) and 3(c). The only indication that a CH_2 species may form upon $-CH_3$ decomposition is from the frequency shift of the C-H stretching mode from 2990 to 2920 cm^{-1} [Fig. 3 (b-c)].

As shown in Fig. 4, the symmetric and asymmetric $=CH_2$ stretching modes are lower in frequency by 30 - 40 cm^{-1} than for those of $-CH_3$ [22,23]. Similarly, the downward shift (~70 cm^{-1}) of the C-H stretching frequency as CH_3 species are heated to 700 K [Figs. 3(b-c)] may suggest that $-CH_2$ species are being formed near 700 K at the expense of adsorbed CH_3 species on the surface. Another explanation for this apparent frequency shift is that changes in the adsorbate bonding geometry of the CH_3(a) species cause the symmetric and asymmetric components of the CH_3 stretch to change in relative intensity [25]. However, we do not believe this to be the cause of the observed frequency shift since the simultaneous intensification of the Si-H stretch (2140 cm^{-1}) in the temperature range 600 - 700 K reveals $-CH_3$ decomposition. After heating to 775 K, when only adsorbed -CH remains, the ν(CH) frequency appears at 2970 cm^{-1}. A mixture of $-CH_3$ and -CH would not be expected to produce a 2920 cm^{-1} C-H stretch. It seems reasonable to propose that the species causing the lower C-H frequency (2920 cm^{-1}) differs from either the $-CH_3$ or the CH species. Therefore, we propose that by 700 K the adsorbed $-CH_3$ species begin to dissociate into CH_2(a) and CH(a), as indicated by the appearance of hydrogen on the silicon surface, by the emergence of a new δ(C-H) band between 945 - 980 cm^{-1}, and by the 70 cm^{-1} reduction in the C-H stretching frequency to 2920 cm^{-1} upon heating to 700 K.

Heating to temperatures above 700 K causes the desorption of I and D_2 from CD_3I/Si(100) above 700 K [Figs. 2(a) and 2(c)]. The desorption of I by 850 K, and the simultaneous removal of the 425 cm^{-1} loss observed by HREELS [Fig. 3(e)] confirms our previous assignment of this band as the Si-I stretching mode. Also observed by TPD and HREELS is the removal of adsorbed D(H) from the Si surface.

TPD shows the desorption of D_2 (mass 4) from CD_3I/Si(100) at a peak temperature of 785 K [Fig. 2(c)]. Correlating to this desorption process is the loss of the Si-H vibrational feature from CH_3I/Si(100) at 2140 cm^{-1} upon heating [Compare Figs. 2(c) and 3(e)].

By 850 K only a 770 cm^{-1} vibrational loss remains which is due to carbon on the surface [26]. The presence of adsorbed carbon on the surface after heating to 850 K is verified by AES.

IV. Summary

A method has been found for the production of adsorbed CH_3 species on Si(100), using the dissociative adsorption of CH_3I. A low exposure of 1.5 x 10^{14} CH_3I/cm^2 adsorbs dissociatively on the Si(100)-(2x1) surface at 100 K as CH_3(a) and I(a) species, with a small amount of co-adsorbed molecular CH_3I. Higher exposures (~1 x 10^{15} CH_3I/cm^2) form a molecularly condensed overlayer which exhibits a vibrational spectrum characteristic of the undissociated CH_3I species. The CH_3(a) species produced upon adsorption at 100 K is shown by HREELS to be thermally stable to 600 K; above 600 K it begins to decompose to CH(a), possibly via the production of CH_2(a) species. By 775 K only CH(a), H(a) and I(a) remain on the surface. A carbon-covered Si(100) surface remains after heating to 900 K. TPD studies of higher coverages of CD_3I from Si(100)-(2x1) show two CD_3I desorption features: a low temperature molecular desorption peak at 225 K from weakly-bound CD_3I, and a broad CD_3I desorption feature which extends to ~ 500 K. At higher temperatures I and D_2 are observed to desorb from the surface between 650 - 850 K and 725 - 875 K, respectively.

V. Acknowledgments

We gratefully acknowledge support of this work by the Air Force Office of Scientific Research (AFOSR) under contract number F4962084C-0063.

References

[1] C.T. Rettner, H.E. Pfnür, H. Stein and D.J. Auerbach, J. Vac. Sci. Technol. A6 (1988) 899, and references therein.

[2] S.T. Ceyer, Langmuir 6 (1990) 82.

[3] M.B. Lee, Q.Y. Yang and S.T. Ceyer, J. Chem. Phys. 87 (1987) 2724.

[4] G.R. Schoffs, C.R. Arumainayagam, M.C. McMaster and R.J. Madix, Surface Sci. 215 (1989) 1.

[5] B. Roop, K.G. Lloyd, S.A. Costello, A. Campion and J.M. White, J. Chem. Phys. 91 (1989) 5103.

[6] Z.-M. Lui, S.A. Costello, B. Roof, S.R. Coon, S. Akhter and J.M. White, J. Phys. Chem. 93 (1989) 7681.

[7] K.A. Trentelman, H. Fairbrother, P.C. Stair, P.G. Strupp and E. Weitz, J. Vac. Sci. Technol. A9 (1991) 1820.

[8] G. Radhakrishnan, W. Stenzel, H. Conrad and A.M. Bradshaw, Appl. Surface Sci. 46 (1990) 36.

[9] J.G. Chen, T.P. Beebe, Jr., J.E. Crowell and J.T. Yates, Jr., J. Amer. Chem. Soc. 109 (1987) 1726.

[10] F. Zaera, AVS Abstracts (1992), p. 312.

[11] G.H. Smudde, Jr., X.D. Peng, R. Viswanathan and P.C. Stair, J. Vac. Sci. Technol. A9 (1991) 1885.

[12] H. Gutleben, S.R. Lucas, C.C. Cheng, W.J. Choyke and J.T. Yates, Jr. Surface Sci. 257 (1991) 146.

[13] M.A. Rueter and J.M. Vohs, J. Vac. Sci. Technol. A 9 (1991) 2916.

[14] T.M. Gentle, P. Soukiassian, K.P. Schuette, M.H. Bakshi and Z. Hurych, Surface Sci. 202 (1988) L568.

[15] F. Lee, A.L. Backman, R. Lin, T.R. Gow and R.I. Masel, Surface Sci. 216 (1989) 173.

[16] J.E. Crowell, J.G. Chen and J.T. Yates, Jr., Surface Sci. 165 (1986) 37.

[17] P.J. Chen, M.L. Colaianni and J.T. Yates, Jr., J. Vac. Sci. Technol. A8 (1990) 764.

[18] R.M. Wallace, C.C. Cheng, P.A. Taylor, W.J. Choyke and J.T. Yates, Jr., Appl. Surface Sci. 45 (1990) 201.

[19] R.C. Henderson, J. Electrochem. Soc. 119 (1972) 772.

[20] M.J. Bozack, L. Muehlhoff, J.N. Russell, Jr., W.J. Choyke and J.T. Yates, Jr., J. Vac. Sci. Technol. A 5 (1987) 1.

[21] R. Shimanouchi, Tables of Molecular Vibrational Frequencies, Consolidated Vol. I. U.S. Government Printing Office : Washington, D.C., 1972.

[22] R.T. Conley, Infrared Spectroscopy, Allyn and Bacon, Inc., Boston, 1972.

[23] L.J. Bellamy, The Infrared Spectra of Complex Molecules, John Wiley and Sons, New York, 1975.

[24] H. Froitzheim, The Chemical Physics of Solid Surfaces and Heterogeneous Catalysis, Vol. 5, Eds. D.A. King and D.P. Woodruff, Elsevier, New York, 1988, Ch. 5.

[25] H. Ibach and D.L. Mills, Electron Energy Loss Spectroscopy and Surface Vibrations, Academic Press, New York, 1982.

[26] J.A. Stroscio, S.R. Bare and W. Ho, Surface Sci. 154 (1985) 35.

[27] A.L. Smith, J. Chem. Phys. 21 (1953) 1997.

[28] D.C. McKean, G. Davidson and L.A. Woodward, Spectrochim. Acta 26A (1970) 1815.

[29] J. Yoshinobu, H. Tsuda, M. Onchi and M. Nishijima, J. Chem. Phys. 87, (1987) 7332.

[30] J.E. Demuth and H. Ibach, Surface Sci. 78 (1978) L747.

Figure Captions

Figure 1. Vibrational spectra of submonolayer (A) and multilayer (B) coverages of CH_3I on a Si(100)-(2x1) surface at 100 K (a), and after heating to 200 K for one minute (b).

Figure 2. Temperature programmed desorption spectra of ~2.4 x 10^{15} CD_3I/cm^2 adsorbed onto Si(100)-(2x1) at 130 K. The heating rate employed was 1 K/s.

Figure 3. Vibrational spectra of CH_3I adsorbed on Si(100)-(2x1) at 300 K, followed by sequential heating to the indicated temperature (1 K/s). All spectra were recorded after cooling to 100 K.

Figure 4. A schematic of the infrared spectral region where C-H stretching frequencies are typically observed. From ref. 22.

Table I. Vibrational Assignments

CH_3I(a)	(cm^{-1})	
Mode	Si(100)[a]	CH_3I(g)[b]
$\nu_{as}(CH_3)$	3080	3060
$\nu_s(CH_3)$	3000(sh)	2970
$\delta_a(CH_3)$	1425	1436
$\delta_s(CH_3)$	1250	1252
$\rho(CH_3)$	900	882
ν(C-I)	525	533

CH_3(a)	(cm^{-1})		
Mode	Si(100)[a]	Si(100)[c]	Cl_3SiCH_3[d]
$\nu_{as}(CH_3)$	2990	3000	2990
$\nu_s(CH_3)$	~2930(sh)	2930	2923
$\delta_a(CH_3)$	1425	1450	1417
$\delta_s(CH_3)$	1260	1170	1271
$\rho(CH_3)$	710	690	804

CH_2(a)	(cm^{-1})		
Mode	Si(100)[a]	$(H_3Si)_2CH_2$[e]	C_2H_4/Si(100)[f]
$\nu_{as}(CH_2)$	~2970(w)(sh)	2941	3080(w)
$\nu_s(CH_2)$	2920(s)	2902	2955(s)
$\delta_{sc}(CH_2)$	---(u)	1363	1440
$\tau(CH_2)$	---(u)	1101	----(u)
$\omega(CH_2)$	---(u)	1053	1260
$\rho(CH_2)$	---(u)	776	900

CH(a)		(cm^{-1})		
Mode	Si(100)[a]	Si(100)[g]	Ni(111)[h]	Al(111)[i]
ν(CH)	2970	2980	2980	2930
δ(CH)	945	900	790	760

References

(a) this work (d) ref. 27 (g) ref. 15 (u) unassigned (sh) = shoulder

(b) ref. 21 (e) ref. 28 (h) ref. 30 (s) strong

(c) ref. 13 (f) ref. 29 (i) ref. 9 (w) weak

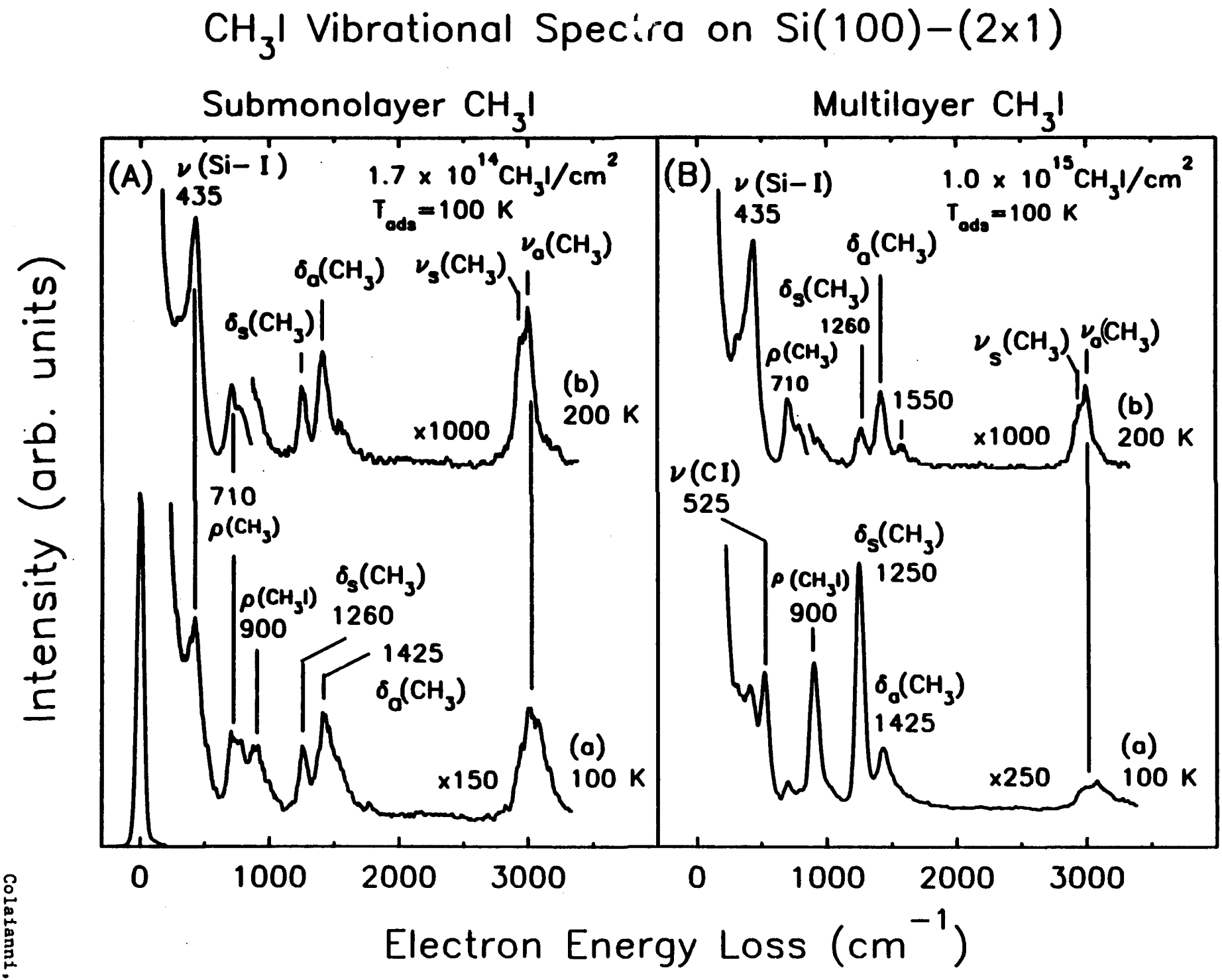

Colaianni, et al.

Figure 1

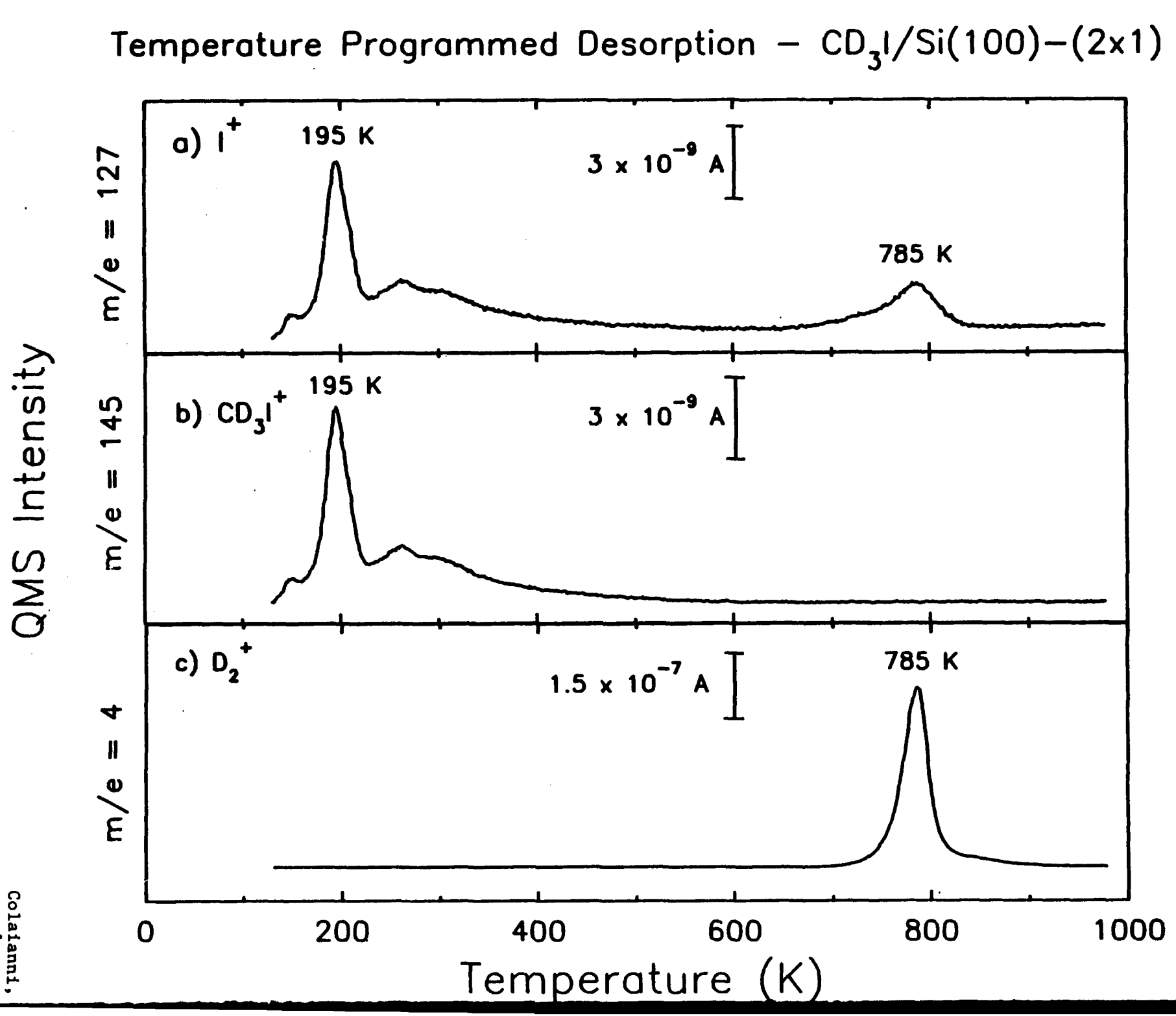

Colaianni, et al.
Figure 2

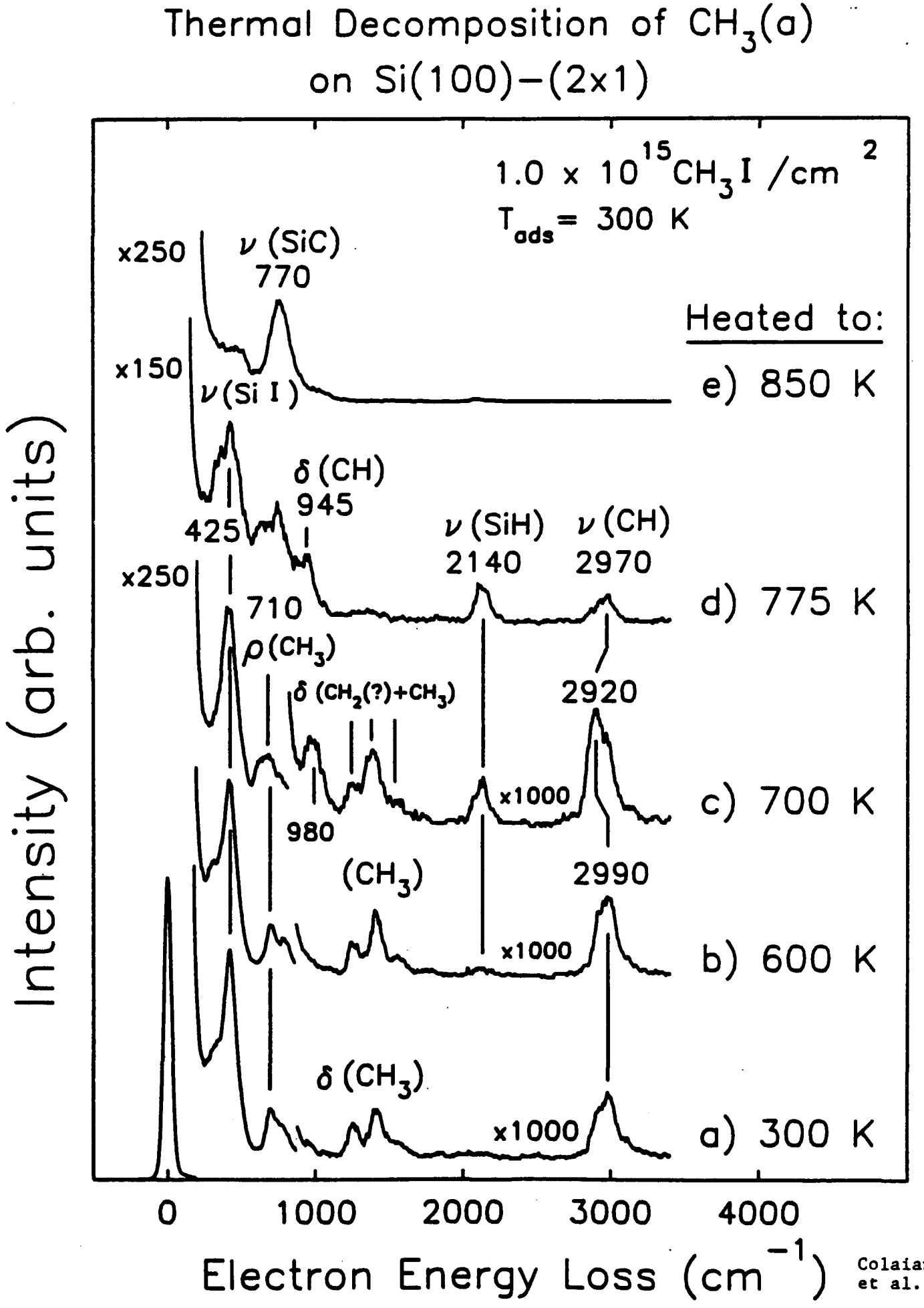

Colaianni, et al.

Figure 3

Typical C-H Vibrational Frequencies

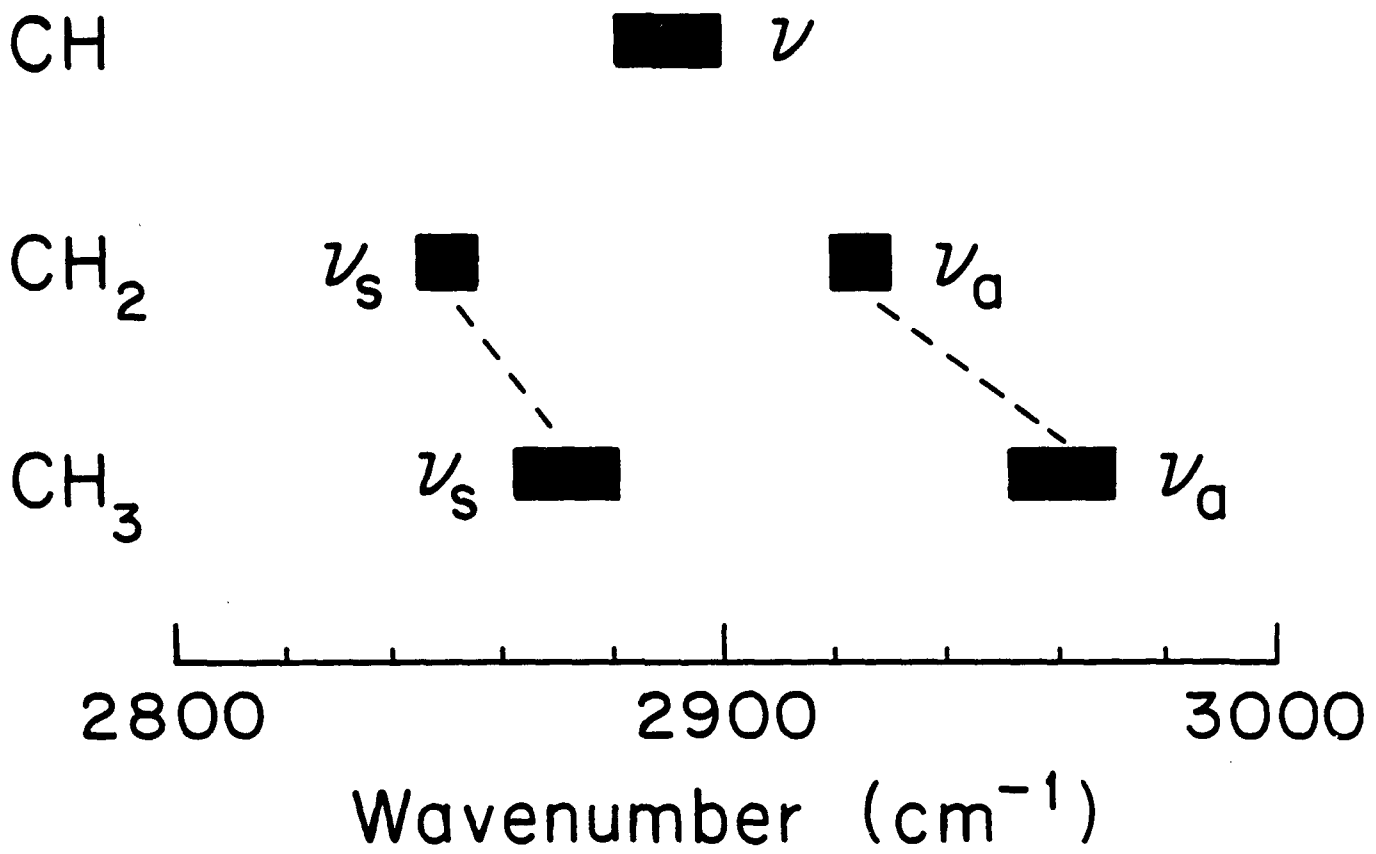

Colaianni, et al.

Figure 4